Full Wavefield Inversion of Ambient Seismic Noise

submitted to *Geophys. J. Int.*

Full Wave Field Inversion of Ambient Seismic Noise

S.A.L. de Ridder[1] and J.R. Maddison[1]

[1] *School of Mathematics and Maxwell Institute for Mathematical Sciences,*

University of Edinburgh, Edinburgh EH9 3FD, United Kingdom.

E-mail: s.deridder@ed.ac.uk

Received March 1, 2018; in original form March 1, 2018

SUMMARY

We formulate a full wave field inversion for ambient seismic noise recorded by large and dense seismograph arrays. Full wave field inversion exploits the constraints on the gradients of the wave field that array data inherently possess. We pose full wave field inversion as a partial differential equation (PDE) constrained inverse problem resulting in a joint estimation of a reconstructed wave field and the medium parameters. The inverse problem is solved by variable projection. We explicitly allow for non-unique solutions to the PDE system that is imposed as a constraint. The boundary conditions of the wave field do not need to be specified, and can remain unknown. This makes the algorithm suitable for inverting observations of ambient seismic noise by dense arrays. The result is that the inverse problem for subsurface properties becomes insensitive to the character and distribution of the noise sources that excited the seismic wave field. In principle the formulation holds equally for ambient noise wave fields and for wave fields excited by controlled sources. The theory is supported with examples in one dimension in the time domain, and in two dimensions in the frequency domain. The latter are of interest in the inversion of surface wave ambient noise for phase velocity maps.

Key words: Inverse theory; Surface waves and free oscillations; Seismic noise; Theoretical seismology; Computational seismology.

1 INTRODUCTION

Our seismological goal is to estimate a set of parameters (e.g. velocity or elasticity) characterising a medium, that allow for the best fit of a predicted wave field and an observed wave field. When inverting for wave forms in controlled source seismic data, this is known as waveform inversion. A predicted wave field is usually obtained by forward modeling using an estimate of the medium parameters. The misfit, computed as the difference between the predicted and observed data, is projected onto the model parameter space to find an update for the model parameters (Tarantola 1984). This procedure is relatively straightforward for controlled source seismic because we know the seismic source positions and excitation functions, and we limit computation to a domain for which we know the boundary conditions. Under those conditions, the partial differential equation (PDE) controlling the wave field has a unique solution. The back projection of misfit between observed and predicted data to an update of the medium parameters relies on the Born linearisation to relate the wave field linearly with the medium parameters. This procedure is not immediately suitable for inverting ambient seismic data, because the noise sources exciting the wave field and other boundary conditions of the medium (e.g. absorbing, reflecting, vanishing) are unknown and therefore we cannot simulate the wave field using an estimate for the medium parameters.

It has long been known that the spatial gradients of seismic wave fields yield information on local medium properties (Curtis & Robertsson 2002; Langston 2007; Liang & Langston 2009; Poppeliers et al. 2013; Liu & Holt 2015; Zhan et al. 2018). Recently, it has been found that spatial gradients can be utilized to infer wave velocities even from ambient seismic noise wave fields (de Ridder & Biondi 2015; Edme & Yuan 2016; de Ridder & Curtis 2017). Here, we show that this relationship can be exploited for inverting ambient seismic noise in a wave field inversion formulation.

A theory now known as seismic interferometry predicts that we can estimate Green's functions between two stations (i.e. the controlled source responses) by cross-correlating recordings of ambient seismic noise recorded at these stations (Aki 1957; Claerbout 1968; Wapenaar & Fokkema 2006). This theory holds assuming certain favorable characteristics of the ambient seismic wave field, which are usually described (although not sufficiently complete) as a state of energy equipar-

tition (Lobkis & Weaver 2001; Snieder et al. 2010). Conventional full waveform inversion has been adapted for waveforms obtained by cross-correlating ambient noise. For example by estimating the character of the ambient noise, and correcting the projection of the misfit onto the model parameter space (Tromp et al. 2010). However, significant uncertainty regarding the effect of the character of the ambient noise remains due to trade-off between source distribution and structure (Fichtner 2015).

An alternative avenue for waveform inversion was proposed by van Leeuwen & Herrmann (2013). They proposed to expand the search space using a PDE constrained inversion formulation, which appears to mitigate the challenge that local minima pose during the non-linear inversion process. Their formulation relies on knowing the wave field source terms in, and the boundary conditions on, the wave equation PDE. To find an update for the model parameters at each iteration of the inversion, does not require solving the adjoint state wave equation. Instead, the gradient computation is achieved by a local projection also known as wave equation inversion (WEI) (Curtis & Robertsson 2002).

We formulate a general wave field inversion scheme for ambient seismic wave fields. The critical difficulty in conventional formulations is that given the medium parameters, the wave field can *only* be reconstructed with knowledge of the boundary conditions and the excitation functions. Without such knowledge, as is the case for ambient seismic wave fields, there is no boundary value problem linking the wave field with the medium parameters, but only a singular system defined by an interior partial differential equation. Therefore, any conventional method that requires the ability to reconstruct the wave field directly from (an estimate of) the medium parameters is unsuitable.

We propose PDE constrained inversion for ambient seismic noise. As examples, we use 1D and 2D scalar wave equations. The 2D frequency domain scalar wave equation (the Helmholtz equation) governs many types of wave fields, including those composed of simple plane waves or an unstructured wave field formed by the superposition of many plane waves, and even standing waves. The Helmholtz equation is relevant for modeling far field behavior of single mode surface waves in laterally homogeneous (or weakly inhomogeneous) media (Aki & Richards 2002).

We use this dispersive Helmholtz equation as a PDE constraint in a joint inverse problem. We invert sparse observations of a wave field jointly for the complete wave field best fitting our observations, and the medium parameters that provide an optimal fit. The uncertainty in the seismic noise source distribution is excluded from the inverse problem by restricting the inversion to a domain in which we can assume (or know) that the sources can be neglected. Boundary conditions on the wave field are explicitly omitted from the PDE system, but are implicitly recovered during the inversion.

The formulation we arrive at is similar as the approach of van Leeuwen & Herrmann (2013), except for some critical key differences in the inverse problem definition. van Leeuwen & Herrmann (2013) formulated an inverse approach inverting for the medium parameters while simultaneously reconstructing the wave field. The optimisation is defined by minimising a combination of a data fitting penalty and an additional PDE residual penalty (at each iteration of the non linear optimisation the PDE need not be perfectly satisfied). Their formulation implies that the PDE residual is well defined everywhere, which requires that the excitation functions of the wave field and its boundary conditions are completely specified. This would be unsuitable for inverting ambient seismic noise recordings.

We resolve this issue by applying the PDE constraint only on the interior of the domain, i.e. we apply a PDE constraint which does not in itself form a well-posed problem. The formulation of the PDE constraint explicitly excludes boundary conditions on the wave field. While the boundary conditions need not be specified explicitly as part of the optimisation process, a set of boundary conditions consistent with the recordings in the interior emerge implicitly at the end of the optimisation procedure. Moreover, by allowing a non-zero PDE residual, the formulation further implicitly inverts for interior sources.

The semantic choice of wave field inversion, as opposed to waveform inversion, in the title reflects that we aim to invert wave fields that can be unstructured, i.e. in which individual waveforms cannot be identified and tracked while propagating over several wavelengths.

2 SEISMOLOGICAL INVERSE PROBLEM

A generalized seismological inverse problem aims to find a wave field, and associated medium parameters, which most closely match a given series of observations made at discrete observation points. Depending on how many observations are available, and how much prior information is available, the seismological inverse problem may be ill-posed with multiple possible solutions which all independently match the observations as closely as possible.

Here the seismological inverse problem is formulated by constructing an appropriate general Lagrange constrained optimisation problem, which is then discretised. The key principles are summarised, but for full technical details see Appendix A. The general inverse problem is formulated by defining

$$\mathcal{L}\left(u, m, s, \lambda\right) = E_u\left(u\right) + E_m\left(m\right) + E_s\left(s\right) - \Big\langle \lambda, \mathcal{F}\left(u, m\right) - s \Big\rangle_{L^2}. \tag{1}$$

Here u is the wave field, m the medium parameters, s the excitation, and λ is a Lagrange multiplier, all of which are functions over space and time. The final term takes the form of an L^2 inner product:

$$\int_\Omega \lambda^* \big(\mathcal{F}\left(u, m\right) - s\big) \mathrm{d}\Omega \tag{2}$$

where the integral is over the solution domain Ω. Complex conjugation is denotes by *. Here, and elsewhere in this article, it is assumed that the relevant fields are real-valued. However this can be generalised for complex-valued fields. The real functions E_u, E_m and E_s are aggregate penalty terms on the state, medium parameters, and excitation spaces, expressing the mis-match between the fields and given data and expected priors. The optimisation problem is to find stationary points of the function $\mathcal{L}$.

The function $\mathcal{F}$ in Eq. 1 expresses the residuals of one of more homogeneous partial differential equations for the wave-field u given the medium parameters m. Boundary conditions can be introduced through appropriate choices of search spaces for u and λ, and through the definition of $\mathcal{F}$. If boundary conditions are specified and the resulting problem is well-posed then seeking stationary points of $\mathcal{L}$ is equivalent to solving the seismological inverse problem via standard adjoint

based methods (e.g. Wunsch 2006). However, boundary conditions can be entirely removed from the problem through a careful choice of search space for λ, in particular by insisting that λ vanishes appropriately on the boundary, so that the Lagrange multiplier applies only the interior partial differential equations as a constraint. In the discrete case, this is achieved by removing equations associated with the boundary conditions from consideration, while still allowing the wave field on the boundary to influence interior equations, and hence influence $\mathcal{L}$.

Seismic properties are generally inferred from a discrete number of seismic observations and a discrete number of experiments, potentially combined with a number of geological observations (e.g. from well logs). Therefore each of the aggregate penalty terms in Eq. 1 will typically include a sum of a data mis-match norm, and a prior information mis-match norm, taking the form (here for E_u, but similarly for E_m and E_s)

$$E_u(u) = \frac{1}{2N_u}\left\|\boldsymbol{\epsilon}_{u,d}\left[\Pi_u(u) - \mathbf{u}_d\right]\right\|_2^2 + \frac{1}{2}\left\|\epsilon_{u,p}\left[u - u_p\right]\right\|_{L^2}^2 + \dots \tag{3}$$

The first term incorporates observations, and the second term incorporates prior information. The addition of such terms play the role of a prior in a Bayesian formulation of inverse problems (Tarantola 2005). Here, the 2-norm is the Euclidean vector norm, and the L^2 norm is defined as $\|\phi\|_{L^2} = \sqrt{\int_\Omega \phi^2}$ (i.e. an appropriate norm for suitable functions in the solution domain Ω).

Further terms of a similar form can be added to each of the aggregate penalty terms E_u, E_m and E_s. Π_u, Π_m, and Π_s are 'sampling operators' which evaluate the state, model, and excitation fields at respectively N_u, N_m, and N_s observation locations. Data vectors $\mathbf{u}_d$, $\mathbf{m}_d$, and $\mathbf{s}_d$ contain observations of the state, model, and excitation fields at these locations. The first term in Eq. 3 contains a factor $\boldsymbol{\epsilon}_{u,d}$ (either a non-negative scalar, or a positive semi-definite matrix) expressing the relative importance of the observations, or incorporating covariance information for the observations. $\epsilon_{u,p}$ (a non-negative scalar or function) selectively samples regions of the domain in the incorporation of prior information.

The second term in Eq. 3 is a form of zeroth order Tikhonov regularisation (Aster et al. 2005). Alternative forms for this second term can be chosen for higher order regularisation. For example, a common prior is that medium parameters should vary smoothly as a function of space. In that

case the term incorporating prior information can take the form

$$E_m(m) = \ldots + \frac{1}{2}\left\|\epsilon_{m,p}\nabla^2 m\right\|_{L^2}^2 + \ldots, \tag{4}$$

which is known as second order Tikhonov regularisation.

3 FULL WAVE INVERSION

The primary emphasis of this article is on the solution of problems for which boundary condition information is unknown. However, the general formulation is first briefly related to novel approaches appearing in the literature, for which boundary conditions *are* specified. In this section we omit observations and prior information on the model parameters, and thus for simplicity consider a Lagrange constrained function of the form

$$\begin{aligned}\mathcal{L}(u,m,s,\lambda) = \\ \frac{1}{2N_u}\left\|\boldsymbol{\epsilon}_{u,d}\left[\Pi_u(u) - \mathbf{u}_d\right]\right\|_2^2 + \frac{1}{2N_s}\left\|\boldsymbol{\epsilon}_{s,d}\left[\Pi_s(s) - \mathbf{s}_d\right]\right\|_2^2 + \frac{1}{2}\left\|\epsilon_{u,p}\left[u - u_p\right]\right\|_{L^2}^2 + \frac{1}{2}\left\|\epsilon_{s,p}\left[s - s_p\right]\right\|_{L^2}^2 \\ -\left\langle \lambda, \mathcal{F}(u,m) - s\right\rangle_{L^2}.\end{aligned} \tag{5}$$

If the partial differential equations defined via $\mathcal{F}$ are supplemented with appropriate boundary conditions, so that a well-posed problem is defined, then there exists a unique function $\mathcal{F}^{-1}$ expressing the solution for the wave field given the medium parameters and excitation functions. That is, in this case there exists a unique function $\mathcal{F}^{-1}$ such that

$$\left\langle \lambda, \mathcal{F}\left(\mathcal{F}^{-1}(m,s), m\right) - s\right\rangle_{L^2} = 0, \tag{6}$$

for all Lagrange multipliers λ in the Lagrange multiplier search space. The key difficulty that is resolved in this article is that the partial differential equation for the wave field cannot be solved in this way for recordings of ambient seismic wave fields with unknown boundary conditions. First, we briefly review existing full waveform inversion strategies.

The objective functions in the remainder of this section may depend on m either through $\mathcal{F}^{-1}(m,s)$ or $\mathcal{F}(u,m)$. The dependence via $\mathcal{F}^{-1}(m,s)$ is commonly linearized by single scattering Born approximation (Hudson & Heritage 1981) and the adjoint projection or full inversion of the objective function residual to a model parameter update is known as respectively reverse time

migration (Baysal et al. 1983) and least squares migration (LeBras & Clayton 1988). The dependence through $\mathcal{F}(u,m)$ is intrinsically linear and the projection of the objective function residual to a model parameter update is known as wave equation inversion (WEI) (Curtis & Robertsson 2002; de Ridder & Biondi 2015; de Ridder & Curtis 2017).

3.1 Conventional full wave form inversion

With no prior information on the wave field, $\epsilon_{u,p} = 0$, and if s is perfectly known everywhere, the search space is commonly restricted such that $s - s_p = 0$ identically and always. Eq. 5 reduces to

$$\mathcal{L}(u,m,s_p,\lambda) = \frac{1}{2N_u}\left\|\boldsymbol{\epsilon}_{u,d}\left[\Pi_u(u) - \mathbf{u}_d\right]\right\|_2^2 - \left\langle \lambda, \mathcal{F}(u,m) - s_p \right\rangle_{L^2}. \tag{7}$$

If a unique $\mathcal{F}^{-1}$ as described above exists then we can define a new function $\widehat{\mathcal{L}}$ with

$$\widehat{\mathcal{L}}(m) = \frac{1}{2N_u}\left\|\boldsymbol{\epsilon}_{u,d}\left[\Pi_u\left(\mathcal{F}^{-1}(m,s_p)\right) - \mathbf{u}_d\right]\right\|_2^2, \tag{8}$$

where a stationary point m_0 of $\widehat{\mathcal{L}}$ corresponds to a stationary point $(\mathcal{F}^{-1}(m_0,s_p), m_0, s_p, \lambda_0)$ of $\mathcal{L}$ for some λ_0. Hence the optimisation problem, seeking stationary points of $\mathcal{L}$, can be reduced to the problem of seeking stationary points of the new function $\widehat{\mathcal{L}}$. This is the classical inversion method, see Plessix (2006) for a review. Usually, seismic records of individual shots are not recorded continuously, and the objective function $\widehat{\mathcal{L}}$ is summed over controlled source experiments. The gradient of the objective function with respect to the medium parameters, commonly named the sensitivity kernel, is obtained as the Jacobian of the misfit function under the norm.

This approach is adapted for inverting the waveforms in noise-correlations. The observed wave field is replaced with the cross-correlation function between two stations, and the forward model predicts that cross-correlation function as a function of noise source distribution and strength, and medium parameters (Tromp et al. 2010). The locations of the noise sources need to be known, or their spatial distribution and strength adequately characterized. These are then used to simulate the generating wave field at the receivers which are cross-correlated to obtain the predicted waveforms.

3.2 Inversion for both the structure and the source functions

Location specific excitation information can be incorporated by restricting the excitation s to be a linear combination of known functions which are localized to specific controlled source locations. I.e., $s = \sum_{i=1}^{N_s} \tilde{s}_i \xi_i$, where ξ_i are given functions of space, and $\tilde{s}_i$ are unknown functions of time to be solved for. This includes a scenario where we discretise the space-time source function on a regular grid covering the entire domain, although this may result in a problem with unresolved trade off between source functions and structure.

If no further prior information on the excitation is provided, and if further prior information on the state parameters is removed. Eq. 5 reduces to

$$\mathcal{L}(u, m, s, \lambda) = \frac{1}{2N_u} \left\| \boldsymbol{\epsilon}_{u,d} \left[\Pi_u(u) - \mathbf{u}_d \right] \right\|_2^2 + \frac{1}{2N_s} \left\| \boldsymbol{\epsilon}_{s,d} \left[\Pi_s(s) - \mathbf{s}_d \right] \right\|_2^2 - \left\langle \lambda, \mathcal{F}(u, m) - s \right\rangle_{L^2}. \quad (9)$$

If a unique $\mathcal{F}^{-1}$ as described above exists then we can define a new function $\widehat{\mathcal{L}}$ with

$$\widehat{\mathcal{L}}(m, s) = \frac{1}{2N_u} \left\| \boldsymbol{\epsilon}_{u,d} \left[\Pi_u \left(\mathcal{F}^{-1}(m, s) \right) - \mathbf{u}_d \right] \right\|_2^2 + \frac{1}{2N_s} \left\| \boldsymbol{\epsilon}_{s,d} \left[\Pi_s(s) - \mathbf{s}_d \right] \right\|_2^2 \quad (10)$$

where a stationary point (m_0, s_0) of $\widehat{\mathcal{L}}$ corresponds to a stationary point $\left(\mathcal{F}^{-1}(m_0, s_0), m_0, s_0, \lambda_0\right)$ of $\mathcal{L}$ for some λ_0. Hence the optimization problem for waveform inversion with an unknown source function, seeking stationary points of $\mathcal{L}$, can be reduced to the problem of seeking stationary points of the new function $\widehat{\mathcal{L}}$. Rickett (2013) tackles that problem using variable projection.

Sager et al. (2018) expanded the inversion strategy for cross-correlation waveforms to include inversion for the noise source distribution. Their approach breaks almost entirely with the mantra to cross-correlate seismic noise in order obtain estimated Green's functions between two station couples. However, they cannot relax the requirement for noise sources to be spatially uncorrelated functions. The inversion for the ambient noise sources is limited to estimating their distribution and power spectrum.

3.3 Inversion for structure while reconstructing the full wave field

Without prior information on the state parameters, $\epsilon_{u,p} = 0$, but assuming that we *do* have prior information for the excitation s_p *everywhere* but no observational data for the excitation. Eq. 5

reduces to

$$\mathcal{L}\left(u,m,s,\lambda\right)=\frac{1}{2N_u}\left\|\boldsymbol{\epsilon}_{u,d}\left[\Pi_u\left(u\right)-\mathbf{u}_d\right]\right\|_2^2+\frac{1}{2}\left\|\epsilon_{s,p}\left[s-s_p\right]\right\|_{L^2}^2-\left\langle\lambda,\mathcal{F}\left(u,m\right)-s\right\rangle_{L^2} \tag{11}$$

If it follows that at a stationary point of $\mathcal{L}$ we have $\mathcal{F}\left(u,m\right)=s$ exactly, and if moreover $\epsilon_{s,p}$ is chosen to be a single scalar, Eq. 5 then reduces to

$$\widehat{\mathcal{L}}\left(u,m\right)=\frac{1}{2N_u}\left\|\boldsymbol{\epsilon}_{u,d}\left[\Pi_u\left(u\right)-\mathbf{u}_d\right]\right\|_2^2+\frac{1}{2}\epsilon_{s,p}^2\left\|\mathcal{F}\left(u,m\right)-s_p\right\|_{L^2}^2. \tag{12}$$

where a stationary point (u_0,m_0) of $\widehat{\mathcal{L}}$ corresponds to a stationary point $\left(u_0,m_0,\mathcal{F}\left(u_0,m_0\right),\lambda_0\right)$ of $\mathcal{L}$ for some λ_0. Hence the optimization problem, seeking stationary points of $\mathcal{L}$, can be reduced to the problem of seeking stationary points of the new function $\widehat{\mathcal{L}}$. This is the inversion method of van Leeuwen & Herrmann (2013), where moreover $\boldsymbol{\epsilon}_{u,d}$ was a single scalar and $s_p=0$.

This formulation requires prior information of the excitation *everywhere* and implies that we have spatial and temporal boundary conditions for the wave field. Neither are available in practice, for inversion of recordings of ambient seismic wave fields.

3.4 Inversion without boundary conditions

In order to limit the inversion to only those parts of the domain where we do have information of the excitation functions, and allow for energy to enter the domain from unknown excitation functions outside of the domain, we need to be able to exclude the boundary conditions from the PDE constraint. For example, starting again with

$$\mathcal{L}\left(u,m,s,\lambda\right)=\frac{1}{2N_u}\left\|\boldsymbol{\epsilon}_{u,d}\left[\Pi_u\left(u\right)-\mathbf{u}_d\right]\right\|_2^2+\frac{1}{2}\left\|\epsilon_{s,p}\left[s-s_p\right]\right\|_{L^2}^2-\left\langle\breve{\lambda},\mathcal{F}\left(u,m\right)-s\right\rangle_{L^2}, \tag{13}$$

we now restrict the Lagrange multiplier $\breve{\lambda}$ so that it vanishes appropriately on all domain boundaries (both at initial and final times, and on spatial boundaries). The inversion problem is now constrained only by the interior partial differential equations specified via the function $\mathcal{F}$, and not by any boundary conditions for the wave field.

Eq. 13 indicates that we supply the optimisation scheme with information regarding the observations of the wave field, prior information regarding the sources, and information from the wave

equation up to but (crucially) not including the boundary itself. Any information regarding the wave field on the boundary is then derived implicitly through its influence on the interior, through the interior partial differential equation. The difficulty that we resolve, is that even though the Lagrange multiplier vanishes on all boundaries, we can substitute the PDE constraint into the mismatch norm (over the interior space plus the boundary) for the prior information of the excitation functions.

A simplified function $\widehat{\mathcal{L}}(u,m)$ as derived in the previous section follows, but its derivation is less straightforward. Specifically, note that if $\epsilon_{s,p}$ is non-zero on domain boundaries then it must follow that at a stationary point of Eq. 13, $s = s_p$ on domain boundaries (assuming here that the excitation is sufficiently smooth that it is meaningful to discuss its boundary values). Otherwise, if $\epsilon_{s,p}$ is zero on domain boundaries then the inversion problem is ill-posed, as s may have any boundary value at stationary points of $\mathcal{L}$. In this case one may restrict consideration to any convenient boundary value for s, such as $s = 0$. In either case the boundary values for the excitation are then completely determined. The Lagrange constraint (reached by differentiating Eq. 13 with respect to the Lagrange multiplier) is

$$\left\langle \zeta, \mathcal{F}(u,m) - s \right\rangle_{L^2} = 0, \tag{14}$$

for all ζ in the Lagrange multiplier search space. Since all ζ vanish on the boundary, and the values for s are known on the boundary, this defines an expression for least-squares (L^2 optimal) projection, with s equal to a least-squares projection of $\mathcal{F}(u,m)$ onto the search space for the excitation, subject to the constraint that s has the given boundary values. This is here denoted $s = \Psi_{L^2}(\mathcal{F}(u,m))$. For further technical details and restrictions in the definition of this projection see Appendix A.

Hence we can define a function

$$\widehat{\mathcal{L}}(u,m) = \frac{1}{2N_u}\left\| \boldsymbol{\epsilon}_{u,d}\left[\Pi_u(u) - \mathbf{u}_d\right] \right\|_2^2 + \frac{1}{2}\left\| \epsilon_s\left[\Psi_{L^2}(\mathcal{F}(u,m)) - s_p\right] \right\|_{L^2}^2 \tag{15}$$

where a stationary point (u_0, m_0) of $\widehat{\mathcal{L}}$ corresponds to a stationary point $(u_0, m_0, \mathcal{F}(u_0,m_0), \lambda_0)$ of $\mathcal{L}$ for some λ_0. Hence the optimization problem, seeking stationary points of $\mathcal{L}$, can be reduced

to the problem of seeking stationary points of the new function $\widehat{\mathcal{L}}$.

In Appendices A and B, we further expand on the properties of the projection operator Ψ_{L^2} while discretising the equations and deriving a system of two discrete objective functions. The result is a formulation that excludes the boundary conditions, which are implicitly recovered during optimization. In contrast to the previous methods described earlier in this section, this formulation is suitable for inverting recordings of an ambient seismic wave field for medium properties.

4 DISCRETE SOLUTION & METHOD

In the remainder of the paper we will provide two numerical examples using scalar wave equations in the time and frequency domain. Here, we first provide discretised equations for full wave field inversion of ambient noise using scalar wave equations. In addition to the data and excitation constraints in Eq. 13, we include two penalty terms on the medium parameters penalising deviations from a given 'prior' field m_p, and penalising non-smooth deviations from this prior, and a regularisation penalising the magnitude of the wave field (Appendix A). The cost function in Eq. 15 is now specified as (Eq. 40 in Appendix A):

$$\widehat{\mathcal{L}}\left(u,m\right)=\frac{1}{2N}\left\|\Pi_u\left(u\right)-\mathbf{u}_d\right\|_2^2+\frac{1}{2}\left\|\epsilon_1\Psi_{L^2}\left(\mathcal{F}\left(u,m\right)\right)\right\|_{L^2}^2+\frac{1}{2}\left\|\epsilon_2 u\right\|_{L^2}^2+\frac{1}{2}\left\|\epsilon_3\nabla^2\left[m-m_p\right]\right\|_{L^2}^2 +\frac{1}{2}\left\|\epsilon_4\left[m-m_p\right]\right\|_{L^2}^2, \quad (16)$$

with either the constant density acoustic wave equation (and time/frequency independent medium parameters)

$$\mathcal{F}\left(u,m\right)=m\nabla^2 u-\partial_{tt}u \quad (17)$$

or the frequency domain Helmholtz equation (with frequency dependent velocity)

$$\widetilde{\mathcal{F}}\left(\widetilde{u},\widetilde{m}\right)=\widetilde{m}\nabla^2\widetilde{u}+\omega^2\widetilde{u} \quad (18)$$

We restrict V_u, V_m, and V_s to be subspaces which each have a finite basis. The spatial and temporal derivatives are approximated by central finite differences on a regular structured spatial grid and temporal grid with spacing Δx in each of two spatial dimensions, and spacing Δt in the

time dimension (for a time-domain inversion as in Section 5) Alternatively, if a Galerkin finite element or Galerkin spectral discretisation were to be applied (but not used here), then a discrete version of the optimisation problem described above could be obtained immediately.

In Appendix B, we show that finding a solution to the stationary points of the cost function in Eq. 16 leads to finding the solution of the following constrained least-squared non-linear optimisation problem:

$$\left[\frac{1}{N\Delta t\Delta x^d}\mathbf{K}^T\mathbf{K} + \breve{\mathbf{H}}^T\breve{\boldsymbol{\epsilon}}_1\breve{\mathbf{H}} + \boldsymbol{\epsilon}_2\right]\mathbf{u} = \frac{1}{N\Delta t\Delta x^d}\mathbf{K}^T\mathbf{d} + \breve{\mathbf{H}}^T\breve{\boldsymbol{\epsilon}}_1\mathbf{s}_\mathrm{p} + \boldsymbol{\epsilon}_2\mathbf{u}_\mathrm{p} \tag{19a}$$

$$\left[\breve{\mathbf{I}}\breve{\mathbf{J}}^T\,\mathrm{diag}\left\{\breve{\mathbf{L}}\mathbf{u}\right\}\,\breve{\breve{\boldsymbol{\epsilon}}}_1\,\mathrm{diag}\left\{\breve{\mathbf{L}}\mathbf{u}\right\}\,\breve{\mathbf{J}}\breve{\mathbf{I}}^T + \mathbf{A}^T\boldsymbol{\epsilon}_3\mathbf{A} + \boldsymbol{\epsilon}_4\right]\mathbf{m} = \breve{\mathbf{I}}\breve{\mathbf{J}}^T\,\mathrm{diag}\left\{\breve{\mathbf{L}}\mathbf{u}\right\}\,\breve{\breve{\boldsymbol{\epsilon}}}_1\breve{\mathbf{D}}\mathbf{u} + \boldsymbol{\epsilon}_4\mathbf{m}_\mathrm{p}, \tag{19b}$$

with

$$\breve{\mathbf{H}} = \breve{\mathbf{H}}\left(\mathbf{m}\right) = \breve{\mathbf{I}}\mathbf{H} = \breve{\mathbf{I}}\Big(\mathbf{D} - \mathbf{M}\mathbf{L}\Big) = \breve{\mathbf{D}} - \breve{\mathbf{M}}\breve{\mathbf{L}}, \tag{20}$$

where $\mathbf{K}$ is a matrix that samples the wave field at the observation locations (dimensions $N_{obs} \times n$). The superscript d in Δx^d indicates the number of spatial dimensions in the scalar wave equation uner consideration. Matrix transposition is denoted by the superscript ^{T}. Table 1 gives the description (with dimensionality) of all other matrices. Equations 19a and 19b describe the full non linear problem explicitly excluding boundary conditions on the wave field.

Let there be n points in the full discrete space - time/frequency grid for the wave field. Let the domain within which we enforce the PDE system and reconstruct the wave field consist of p points. The discrete approximation for the wave field, u, has n degrees of freedom, while the discrete approximations for the medium parameters and excitation functions, m and s, have p degrees of freedom. Then there are are $n - p$ points, for which we reconstruct values that act as the boundary conditions in the discretised PDE system. The initial, terminal, and spatial boundary points, which ought to contain the boundary conditions on the wave field, are explicitly excluded from the fitting objective by introducing a boundary exclusion matrix $\breve{\mathbf{I}}$ (Appendix B). This matrix explicitly confines the PDE penalty term in the Lagrange constraint in Eq. 5 to the values of the wave field located within a specific domain.

Although the $n - p$ points in the boundary zone contain reconstructed wave field values, these values may be very poorly constrained, and may be subject to bias from regularization terms.These values may cause spurious results in the wave equation inversion, and therefore we choose to exclude the reconstructed wave field points in the boundary zone from the wave equation inversion. This is achieved by a secondary boundary exclusion matrix, leaving q points in the secondary interior domain. This secondary selection matrix, $\breve{\mathbf{J}}$, excludes the points in the domain for which evaluation of the finite difference stencils in $\mathbf{L}$ acted on the values in the wave field that contained the implicitly inverted initial, terminal, and spatial boundary points. The selection matrix, $\breve{\breve{\mathbf{J}}}$ confines the inversion for medium parameters to a sub domain consisting of q points.

We refer to the matrix operator, $\breve{\mathbf{I}}$, that excludes the wave field boundary conditions as the boundary exclusion mask (or matrix). While we refer to the matrix operator, $\breve{\breve{\mathbf{J}}}$, that selects only the secondary interior domain as the interior selector mask (or matrix). An alternative description of the matrix operators $\breve{\mathbf{I}}$ and $\breve{\breve{\mathbf{J}}}$ is that they can be interpreted as discrete truncation operators. Fig. 1 clarifies the discretetisation scheme, the boundary exclusion mask and the interior selector mask.

Dimensions on grid	$n \times n$	$p \times n$	$q \times n$	$p \times p$	$q \times q$	$n \times 1$	$p \times 1$
wave field, sources, & medium parameters						$\mathbf{u}$, $\mathbf{u}_\mathrm{p}$	$\mathbf{s}_\mathrm{p}$, $\mathbf{m}$, $\mathbf{m}_\mathrm{p}$
boundary exclusion selector		$\breve{\mathbf{I}}$					
interior domain selector			$\breve{\breve{\mathbf{J}}}$				
2^{nd} order derivative in time	$\mathbf{D}$	$\breve{\mathbf{D}} = \breve{\mathbf{I}}\mathbf{D}$	$\breve{\breve{\mathbf{D}}} = \breve{\breve{\mathbf{J}}}\mathbf{D}$				
2^{nd} order derivatives in space	$\mathbf{L}$	$\breve{\mathbf{L}} = \breve{\mathbf{I}}\mathbf{L}$	$\breve{\breve{\mathbf{L}}} = \breve{\breve{\mathbf{J}}}\mathbf{L}$				
medium parameter action	$\mathbf{M} = \breve{\mathbf{I}}^T \mathrm{diag}\{\mathbf{m}\}\breve{\mathbf{I}}$			$\breve{\mathbf{M}} = \mathrm{diag}\{\mathbf{m}\}$			
wave equation operator	$\mathbf{H}$	$\breve{\mathbf{H}} = \breve{\mathbf{I}}\mathbf{H}$					
regularization operator				$\mathbf{A}$			
covariance matrices	$\boldsymbol{\epsilon}_1, \boldsymbol{\epsilon}_2$			$\breve{\boldsymbol{\epsilon}}_1 = \breve{\mathbf{I}}\boldsymbol{\epsilon}_1\breve{\mathbf{I}}^T, \boldsymbol{\epsilon}_3, \boldsymbol{\epsilon}_4$	$\breve{\breve{\boldsymbol{\epsilon}}}_1 = \breve{\breve{\mathbf{J}}}\boldsymbol{\epsilon}_1\breve{\breve{\mathbf{J}}}^T$		

Table 1. Overview of operators, arrays and their dimensions; n equals the total number of space-time gridpoints, p exludes the initial, terminal, and spatial boundary points, q includes only values inside a interor domain.

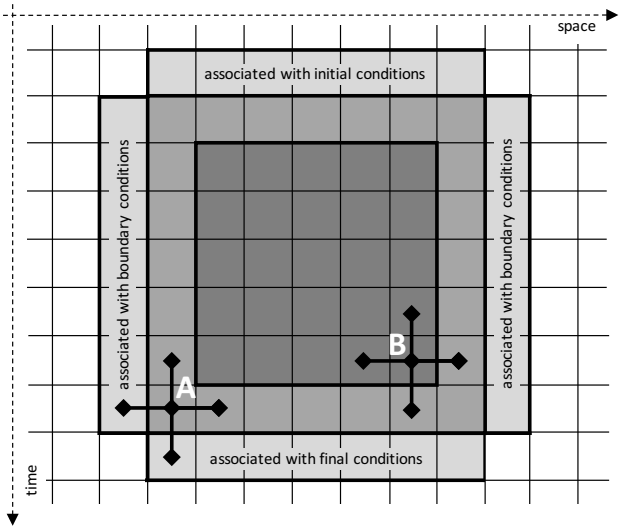

Figure 1. Overview of discretisation scheme for the case of second order finite stencils in space and time: light grey shading indicates the region of n space-time gridpoints (the discrete total domain), medium grey indicates the region of p space-time gridpoints (excluding the the initial, terminal, and spatial boundary points), dark grey includes the region of q space-time gridpoints (the interor domain for wave equation inversion). Stencil A is an example stencil used for wave field reconstruction inversion, and stencil B is an example stencil used for wave equation inversion.

In principle the non-linear Eqs. (19) may be solved via Newton iteration. Given a solution from a previous iteration $(\mathbf{u}_i, \mathbf{m}_i) \in \mathbb{R}^n \times \mathbb{R}^q$ Newton iteration gives the next iteration solution as

$$\begin{pmatrix} \mathbf{u}_{i+1} \\ \mathbf{m}_{i+1} \end{pmatrix} = \begin{pmatrix} \mathbf{u}_i \\ \mathbf{m}_i \end{pmatrix} - \boldsymbol{\mathcal{J}}^{-1}(\mathbf{u}_i, \mathbf{m}_i) \begin{pmatrix} \mathbf{R}_u(\mathbf{u}_i, \mathbf{m}_i) \\ \mathbf{R}_m(\mathbf{u}_i, \mathbf{m}_i) \end{pmatrix}, \tag{21}$$

where the residual functions $\mathbf{R}_u(\mathbf{u}, \mathbf{m})$ and $\mathbf{R}_m(\mathbf{u}, \mathbf{m})$ are associated with Eqs. (19a) and (19b) respectively, and $\boldsymbol{\mathcal{J}}(\mathbf{u}, \mathbf{m})$ is the Jacobian matrix obtained by differentiating the residuals with respect to $\mathbf{u}$ and $\mathbf{m}$. While Newton iteration converges at second order and hence very efficient in terms of the number of iterations required, the full Jacobian matrix $\boldsymbol{\mathcal{J}}(\mathbf{u}, \mathbf{m})$ is of size $(n+p) \times (n+p)$, and hence solving the full coupled problem for both $\mathbf{u}$ and $\mathbf{m}$ in this way may be inefficient.

Here instead, an alternative fixed point iteration method is applied. Given a starting model $\mathbf{m}_i$, a discrete wave field, $\mathbf{u}_{i+1}$, can be found by solving Eq. (19a). Updated discrete medium parameters can be found by solving Eq. 19b for $\mathbf{m}_{i+1}$. This procure is repeated. The second order convergence of full Newton iteration is lost, but the solution procedure on each iteration is

significantly simplified. This is algorithm is expressed as iterating solving for $\mathbf{m}_{i+1}$ in

$$\left[\breve{\mathbf{I}}\breve{\breve{\mathbf{J}}}^T \operatorname{diag}\left\{\breve{\mathbf{L}}\mathbf{G}\left(\mathbf{m}_i\right)\left[\mathbf{f}+\{\breve{\mathbf{H}}\left(\mathbf{m}_i\right)\}^T\breve{\breve{\boldsymbol{\epsilon}}}_1\mathbf{s}_\mathrm{p}\right]\right\}\breve{\breve{\boldsymbol{\epsilon}}}_1 \operatorname{diag}\left\{\breve{\mathbf{L}}\mathbf{G}\left(\mathbf{m}_i\right)\left[\mathbf{f}+\{\breve{\mathbf{H}}\left(\mathbf{m}_i\right)\}^T\breve{\breve{\boldsymbol{\epsilon}}}_1\mathbf{s}_\mathrm{p}\right]\right\}\breve{\breve{\mathbf{J}}}\breve{\mathbf{I}}^T + \mathbf{A}^T\boldsymbol{\epsilon}_3\mathbf{A}+\boldsymbol{\epsilon}_4\right]\mathbf{m}_{i+1} = \tag{22}$$

$$\breve{\mathbf{I}}\breve{\breve{\mathbf{J}}}^T \operatorname{diag}\left\{\breve{\mathbf{L}}\mathbf{G}\left(\mathbf{m}_i\right)\left[\mathbf{f}+\{\breve{\mathbf{H}}\left(\mathbf{m}_i\right)\}^T\breve{\breve{\boldsymbol{\epsilon}}}_1\mathbf{s}_\mathrm{p}\right]\right\}\breve{\breve{\boldsymbol{\epsilon}}}_1\breve{\mathbf{D}}\mathbf{G}\left(\mathbf{m}_i\right)\left[\mathbf{f}+\{\breve{\mathbf{H}}\left(\mathbf{m}_i\right)\}^T\breve{\breve{\boldsymbol{\epsilon}}}_1\mathbf{s}_\mathrm{p}\right]+\boldsymbol{\epsilon}_4\mathbf{m}_\mathrm{p}$$

For convenience we defined the inverse of Eq. 19a as

$$\mathbf{u} = \mathbf{G}\left[\mathbf{f}+\{\breve{\mathbf{H}}\left(\mathbf{m}_i\right)\}^T\breve{\breve{\boldsymbol{\epsilon}}}_1\mathbf{s}_\mathrm{p}\right] \tag{23}$$

with

$$\mathbf{G}=\mathbf{G}(\mathbf{m})=\left[\frac{1}{N\Delta t\Delta x^d}\mathbf{K}^T\mathbf{K}+\{\breve{\mathbf{H}}(\mathbf{m})\}^T\breve{\breve{\boldsymbol{\epsilon}}}_1\breve{\mathbf{H}}(\mathbf{m})+\boldsymbol{\epsilon}_2\right]^{-1} \quad \text{and} \quad \mathbf{f}=\frac{1}{N\Delta t\Delta x^d}\mathbf{K}^T\mathbf{d}+\boldsymbol{\epsilon}_2\mathbf{u}_\mathrm{p} \tag{24}$$

4.1 Practical considerations and simplification

When we can assume that the source functions within a certain domain are zero or can be neglected, we have $\mathbf{s}_\mathrm{p}=\mathbf{0}$. When we remove the mean of each recording, the data has zero mean and a good prior could be $\mathbf{u}_\mathrm{p}=\mathbf{0}$. Furthermore, we choose $\boldsymbol{\epsilon}_1$ such that $\boldsymbol{\epsilon}_1=\breve{\mathbf{I}}^T\breve{\boldsymbol{\epsilon}}_1\breve{\mathbf{I}}=\breve{\mathbf{I}}^T\breve{\mathbf{I}}\boldsymbol{\epsilon}\breve{\mathbf{I}}^T\breve{\mathbf{I}}$, and we define $\boldsymbol{\varepsilon}_1$ such that $\boldsymbol{\varepsilon}_1=\breve{\breve{\mathbf{J}}}^T\breve{\breve{\boldsymbol{\epsilon}}}_1\breve{\breve{\mathbf{J}}}=\breve{\breve{\mathbf{J}}}^T\breve{\breve{\mathbf{J}}}\boldsymbol{\epsilon}\breve{\breve{\mathbf{J}}}^T\breve{\breve{\mathbf{J}}}$. This means that the masking properties are absorbed into $\boldsymbol{\epsilon}_1$ and $\boldsymbol{\varepsilon}_1$. Then all variables can be defined on discrete bases with $p=q=n$, except for in the definitions of $\breve{\mathbf{I}}$ and $\breve{\breve{\mathbf{J}}}$, consequently, we can omit all boundary exclusion masks, and the $\breve{}$ and $\breve{\breve{}}$ over variables, and the mappings $\breve{\breve{\mathbf{J}}}\breve{\mathbf{I}}^T$ and $\breve{\mathbf{I}}\breve{\breve{\mathbf{J}}}^T$ from Eqs. 19a, 19b, and 22 to 24. The notation of the operations then simplifies to

$$\left[\operatorname{diag}\left\{\mathbf{L}\mathbf{G}\left(\mathbf{m}_i\right)\mathbf{f}\right\}\boldsymbol{\varepsilon}_1\operatorname{diag}\left\{\mathbf{L}\mathbf{G}\left(\mathbf{m}_i\right)\mathbf{f}\right\} + \mathbf{A}^T\boldsymbol{\epsilon}_3\mathbf{A}+\boldsymbol{\epsilon}_4\right]\mathbf{m}_{i+1} = \operatorname{diag}\left\{\mathbf{L}\mathbf{G}\left(\mathbf{m}_i\right)\mathbf{f}\right\}\boldsymbol{\varepsilon}_1\mathbf{D}\mathbf{G}\left(\mathbf{m}_i\right)\mathbf{f}+\boldsymbol{\epsilon}_4\mathbf{m}_\mathrm{p} \tag{25}$$

with

$$\mathbf{G}=\mathbf{G}(\mathbf{m})=\left[\frac{1}{N\Delta t\Delta x^d}\mathbf{K}^T\mathbf{K}+\{\mathbf{H}(\mathbf{m})\}^T\boldsymbol{\epsilon}_1\mathbf{H}(\mathbf{m})+\boldsymbol{\epsilon}_2\right]^{-1} \quad \text{and} \quad \mathbf{f}=\frac{1}{N\Delta t\Delta x^d}\mathbf{K}^T\mathbf{d} \tag{26}$$

In the following section we will provide numerical examples and further specify the matrices in these equations for a scalar wave equation in one dimension with time-constant medium properties, and for a scalar wave equation in two dimensions with dispersive medium properties.

5 TIME-DOMAIN EXAMPLE IN 1D

Our first example illustrates full wave field inversion of an unstructured wave field obeying a one-dimensional time-domain scalar wave equation, with time independent medium velocity. We define a new medium parameter with discrete approximation $\widehat{\mathbf{m}}$ on a grid with m points in space. A spraying projection operator $\mathbf{P}$ (dimensions $n \times m$) makes copies of $\widehat{\mathbf{m}}$ for all time-samples: we have $\mathbf{m} = \mathbf{P}\widehat{\mathbf{m}}$. Substitution into Eq. 25 we find

$$\left[\operatorname{diag}\left\{\mathbf{LG}\left(\mathbf{P}\widehat{\mathbf{m}}_i\right)\mathbf{f}\right\} \boldsymbol{\varepsilon}_1 \operatorname{diag}\left\{\mathbf{LG}\left(\mathbf{P}\widehat{\mathbf{m}}_i\right)\mathbf{f}\right\} \; + \mathbf{A}^T\boldsymbol{\epsilon}_3\mathbf{A} + \boldsymbol{\epsilon}_4 \right] \mathbf{P}\widehat{\mathbf{m}}_{i+1} \tag{27}$$

$$= \operatorname{diag}\left\{\mathbf{LG}\left(\mathbf{P}\widehat{\mathbf{m}}_i\right)\mathbf{f}\right\} \boldsymbol{\varepsilon}_1 \mathbf{DG}\left(\mathbf{P}\widehat{\mathbf{m}}_i\right)\mathbf{f},$$

with

$$\mathbf{G} = \mathbf{G}(\mathbf{P}\widehat{\mathbf{m}}) = \left[\frac{1}{N\Delta t \Delta x}\mathbf{K}^T\mathbf{K} + \{\mathbf{H}(\mathbf{P}\widehat{\mathbf{m}})\}^T\boldsymbol{\epsilon}_1\mathbf{H}(\mathbf{P}\widehat{\mathbf{m}}) + \boldsymbol{\epsilon}_2 \right]^{-1} \quad \text{and} \quad \mathbf{f} = \frac{1}{N\Delta t \Delta x}\mathbf{K}^T\mathbf{d}. \tag{28}$$

The temporal derivative matrix $\mathbf{D}$ contains $-2/\Delta t^2$ on it's diagonal, and $1/\Delta t^2$ values spaced m points over. The spatial derivative operator $\mathbf{L}$ contains the central coefficient on its diagonal, immediately flanked by off-center coefficients. The rows corresponding to boundary zone are modified (zeroed) by the definition of $\breve{\mathbf{J}}$ and $\breve{\breve{\mathbf{J}}}$. Inverting this equation results in a least-squares regression with a summation over time-slices (the adjoint of the spraying projection operation is a summation projection operator).

We modeled data from two sources, positioned on either end of an 80 m one dimensional domain, using a finite difference code. The true medium velocity of the simulations is a background velocity of 2000 m/s with, at the center of the domain, a Gaussian anomaly of 200 m/s with a width of approximately 20 m, shown with a blue curve in Fig. 2c. The side reflections were excluded (by extending the model domain), but this was unnecessary because we are only concerned with the wave behavior in the interior. Copies of the two simulated wave fields were added together with random time-delays, and random amplitude multiplication factors, to create the wave field shown in Fig. 2a. This wave field was then sampled to simulate observations of an array with station intervals of 6 m shown in Fig. 2b (the observation locations are shown with blue circles in Fig. 2c). The wave equation operators are constructed with second order accuracy in time and 10^{th} order accuracy in space. The domain for the wave field which we intend to invert for is extended accord-

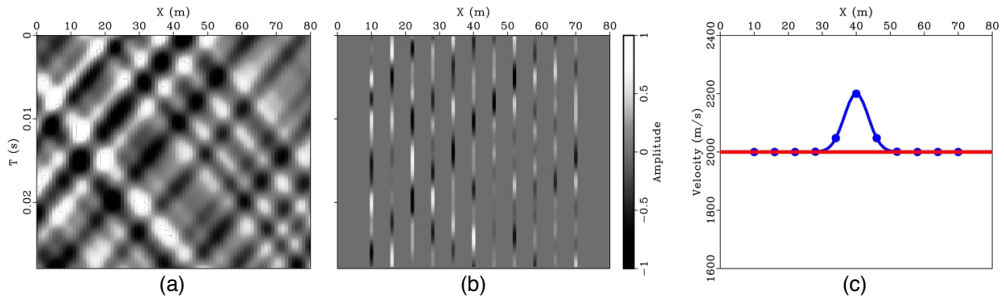

Figure 2. a) A full synthesized wave field (with unitless amplitude) of a series of waves traveling left and right through the true velocity model. b) Sampled wave field (i.e. the data). c) True velocity and observation locations (blue line and blue circles), starting velocity model (red curve).

ingly. The boundary exclusion selector $\breve{\mathbf{I}}$ in the wave field inversion begins at the first observation point and ends at the last observation point. The interior domain selector $\breve{\breve{\mathbf{J}}}$ for WEI excludes 5 additional spatial grid points (on each side), and 1 additional time grid point (at the start and ending time). This way, all wave field values falling in the boundary zone grid points of the wave field, are excluded during WEI.

We invert for the wave field, starting with a homogeneous velocity of 2000 m/s shown by the red curve in Fig. 2c, and find the wave field in Fig. 3a. Through WEI we find the accompanying velocity profile shown by the red curve in Fig. 3e. We repeat the inversion for the wave field and accompanying velocity profile for 10 iterations total (the wave field and velocity profiles after iterations 2, 3, and 10 are shown in Figure 3b to 3d and 3f to 3h).

The difference between the final reconstructed wave field (Fig. 3d) and the true wave field (Fig. 2d) is computed and shown in Fig. 4a. The red dots on the X-axis of Fig. 4a denote the observation locations. Note how the difference is zero at the observation locations. The normalized data misfit (with logarithmic axis) and the normalized change in the model space are shown in Fig. 4b, with respectively red curve with circles, and blue curve with crosses. The data misfit becomes less than 10^{-13} after iteration 4 and is effectively zero.

In this example, we retrieved the correct velocity profile remarkably well. We started our inversion from a velocity profile that was correct near the ends of our array. In the next section, we shall explore the effects of different anomaly sizes, wave field sampling spaces, and erroneous starting velocities.

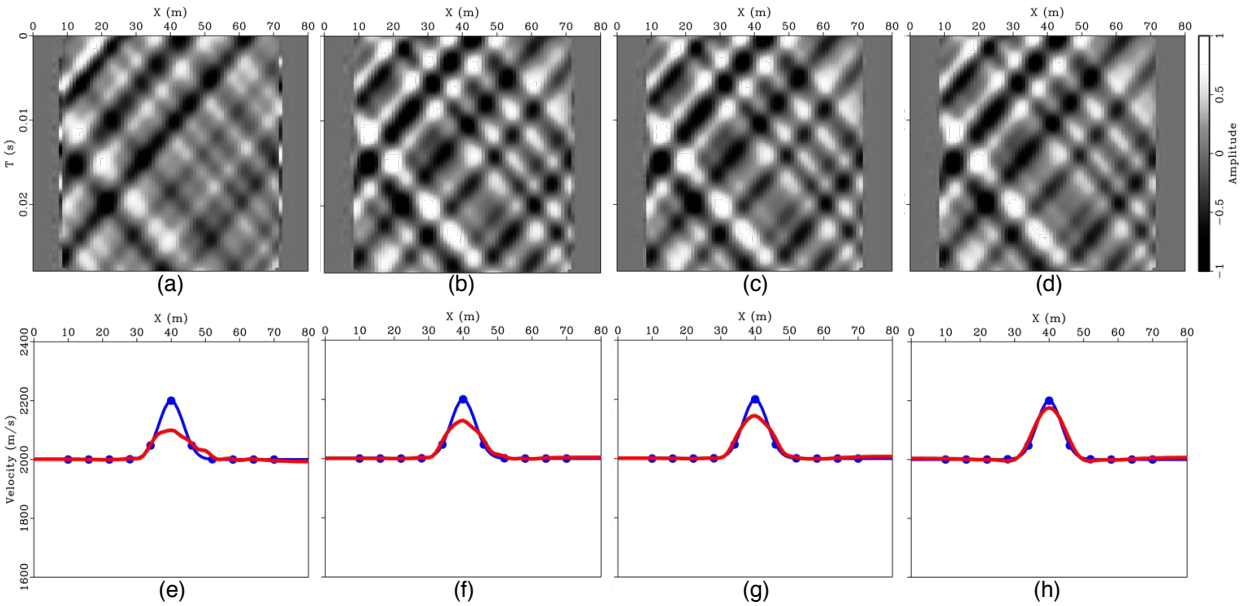

Figure 3. Recovered wave fields (a to d) and recovered velocity models (e to h) in: iteration 1 (a and e); iteration 2 (b and f), iteration 3 (c and g), iteration 10 (d and h).

6 FREQUENCY-DOMAIN EXAMPLE IN 2D

Our second example illustrates full wave field inversion of an unstructured wave field obeying a two-dimensional frequency-domain scalar wave equation. Here, we limit our inversion to a single frequency. In accordance with Parseval's theorem, time and frequency domain inversions are equivalent. The inversion of data from one wave field realization at a specific frequency (a field of complex numbers) should result in the retrieval of the correct medium parameters. However,

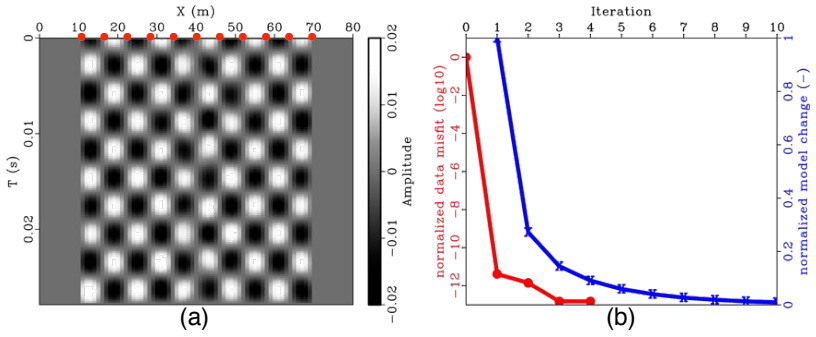

Figure 4. a) Difference between the recovered wave field at iteration 10 (Fig. 2d) and the true wave field (Fig. 3a) within the sample limits in space and time (the domain selected by **I**). Red dots indicate the sampling locations. b) Logarithmic normalized data misfit (red curve) and normalized model change (blue curve) versus iteration.

at points where the complex amplitudes are zero, the medium parameters are not constrained. Therefore, we invert multiple wave field realizations (i.e. multiple experiments) for the same set of medium parameters (i.e. a regression). The specific form of Eq. 25 relevant for this section are

$$\left[\operatorname{diag}\left\{\mathbf{L}\widetilde{\mathbf{G}}\left(\mathbf{m}_i\right)\mathbf{f}_j\right\}\boldsymbol{\varepsilon}_1 \operatorname{diag}\left\{\mathbf{L}\widetilde{\mathbf{G}}\left(\mathbf{m}_i\right)\mathbf{f}_j\right\} + \mathbf{A}^T\boldsymbol{\epsilon}_3\mathbf{A} + \boldsymbol{\epsilon}_4\right]\mathbf{m}_{i+1} \tag{29}$$

$$= \operatorname{diag}\left\{\mathbf{L}\widetilde{\mathbf{G}}\left(\mathbf{m}_i\right)\mathbf{f}_j\right\}\boldsymbol{\varepsilon}_1\widetilde{\mathbf{D}}\widetilde{\mathbf{G}}\left(\mathbf{m}_i\right)\mathbf{f}_j,$$

with

$$\widetilde{\mathbf{G}} = \widetilde{\mathbf{G}}(\mathbf{m}) = \left[\frac{1}{N\Delta x^2}\mathbf{K}^T\mathbf{K} + \{\widetilde{\mathbf{H}}(\mathbf{m})\}^T\boldsymbol{\epsilon}_1\widetilde{\mathbf{H}}(\mathbf{m}) + \boldsymbol{\epsilon}_2\right]^{-1} \quad \text{and} \quad \mathbf{f}_j = \frac{1}{N\Delta x^2}\mathbf{K}^T\mathbf{d}_j, \tag{30}$$

where N is the total number of data sets, $\mathbf{d}_j$, which each are observations of a wave field realization (the regression occurs over the subscript j when solving this system). The matrix with the approximation of the temporal derivative, $\widetilde{\mathbf{D}}$, now simply contains $-\omega^2$ on it's diagonal.

The first test velocity model is 500 m by 500 m, and contains a checker board pattern of anomalies of 300 m/s deviation from a mean velocity of 3000 m/s. The checkers are 75 m wide and are oriented at 45 $^\circ$ with respect to the station geometry (Fig. 5a). The computational domain is somewhat larger then the model-domain shown in Fig. 5a). The mean velocity of the checkers is 3000 m/s, and the average wavelength at the frequency under consideration, $f = 10$ Hz, is 300 m.

We generated synthetic data with a time-domain finite difference code. Data was created for eight sources, positioned at all 4 corners, and half-way along the edges, just outside domain shown in Fig. 5a. Copies of the recordings from all individual sources were mixed together with random time-delays and random amplitudes. The frequency-domain complex amplitudes were computed by Fourier transform at a specific frequency. In order to generate multiple realizations of the experiment, the Fourier Transform was performed in a time window which was moved inside the longer recording generated using the time-domain simulations. The real part of the complex amplitudes of one realization are shown in Fig. 5a.

The first experiment geometry we consider is from an array of 243 stations positioned along lines, spaced 15 m in line and 45 m cross-line. We start our inversions from a homogeneous background velocity of 3500 m/s, which is deviates significantly from the average velocity in the true velocity model. In a first step, we invert for an average background velocity by running

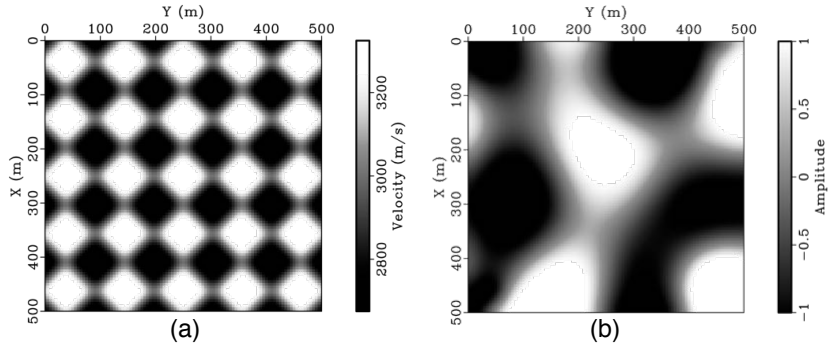

Figure 5. a) Two dimensional velocity model containing a checker board pattern of anomalies of 75 m by 75 m, at a 45 ° angle with respect to the receiver grid . b) The real part of one wave field realization (out of 6000 realizations).

the iterative inversions with a relatively strong regularization enforcing spatial smoothness. In the second step, we invert for the details of the velocity model by relaxing the regularization term and restarting the iterative inversion scheme. The iterations are stopped when the change in the velocity model falls below 0.01 %. Fig. 6 shows this inversion process starting from the velocity model in Fig. 6e. The location of the receivers are indicated in Fig. 6 by red dots, the domain of interest ends immediately outside the square domain that encloses the observations points. Fig. 6a and 6f show the first reconstructed wave field (in step 1) and its accompanying velocity field, Fig. 6b and 6g show the last reconstructed wave field (in step 1) where the iterations in step 1 stopped (iteration 7). Fig. 6c and 6h show the wave field and its accompanying velocity field after the first iteration in step 2, Fig. 6d and 6i show the wave field and its accompanying velocity field after the last iteration in step 2 (iteration 51). Near the edges of the domain of interest, the reconstructed wave field appears spurious, however from the accompanying velocity fields, we see that the wave field near the edges obeys a non-spurious velocity. We will elaborate on this observation in the discussion section. Fig. 7 contains graphs of the the normalized data misfit (red curve) and normalized model change on a logarithmic scale (blue curve), as a function of iteration. The disruption between iteration 7 and 8 is due to the transition from step 1 to step 2. Notice that reducing the regularization strength in step 2 allowed for a smaller data misfit.

In order to gain an initial understanding of the resolution and limitations of the proposed method for wave field inversion, we tested a variety of different wave field sampling densities,

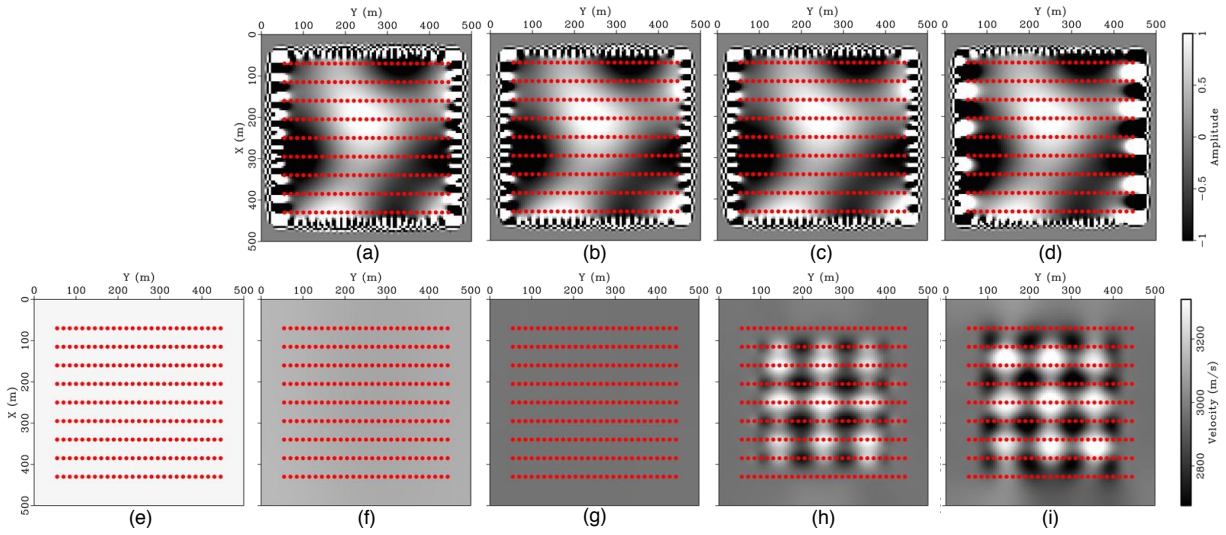

Figure 6. Recovered wave fields and recovered velocity models. The starting velocity model in (e). The first and last iteration of the first iteration series with strong spatial smoothing: wave fields in (a and b) and velocity models in (f and g). The first and last iteration of the second iteration series with weak spatial smoothing: wave fields in (c and d) and velocity models in (h and i). The final recovered velocity model in (i).

and checker sizes. For each model, and acquisition geometry, we performed the same two step inversion as described above. The true velocity models, sampling geometries, and retrieved velocity fields are collected in Fig. 8. The first row contains the true velocity models, and from top to bottom in the remaining four rows the cross-line spacing of the station geometry varies as 15 m, 45 m,

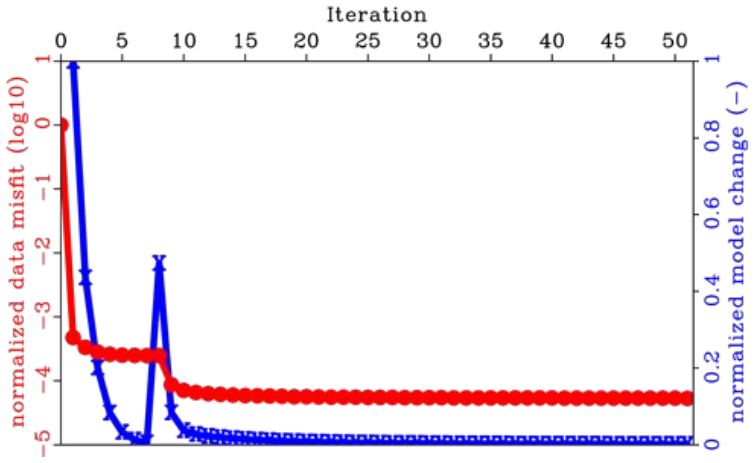

Figure 7. Logarithmic normalized data misfit (red curve) and normalized model change (blue curve) versus iteration. The first iteration series with strong spatial smoothing (iteration number 1 to 7). The second iteration series with weak spatial smoothing (iteration number 8 to 51).

60 m, and 90 m, the in-line spacing is 15 m. In the four columns from left to right, the checker sizes vary as 75 m, 100 m, 125 m, and 150 m, all oriented at 45 °angle with the station geometry. For the velocity model with the largest checkers, and the station geometry with the shortest cross-line spacing, the velocity model is near perfectly retrieved. Whereas for the smallest checkers and the station geometry with the largest cross-line spacing, the retrieved velocity model misses the checkers entirely (bottom-right). Notice that as the station geometry cross-line spacing increases, we are unable to reconstruct the velocity anomalies near the edges of the array. We will further elaborate on this in the next section.

7 DISCUSSION

The core of the inversion method for seismic wave fields outlined in this paper is to impose a PDE system with non unique solutions as a constraint in the seismic inverse problem. We can constrain medium parameters while estimating the wave field, without having to specify or estimate the sources that generate the wave field everywhere in the domain. More specifically, we can separate the inversion for medium parameters in a sub domain in which we have knowledge about the sources, from a larger domain that includes areas where we do not have knowledge of the sources. In the examples presented in this paper, we chose the sources within the sub domain to have a prior of zero.

In most seismic inverse problems, the information on the medium parameters (for example wave-speed) comes from observed travel times between two points in the medium. In this study, the information on medium parameters is extracted with an inversion method operating *locally*, named wave equation inversion (Curtis & Robertsson 2002). This method recognizes that the medium characters can be extracted once the spatial and temporal gradients of a wave field, and local acting sources, are known. Observations made by densely spaced station arrays constrain the spatial and temporal gradients of a wave field.

The examples shown in this paper show how in the interior regions of dense station arrays, the spatial and temporal gradients of a wave field are sufficiently constrained so that they resolve the medium parameters. Given a certain station arrangement and velocity model, certain wave modes

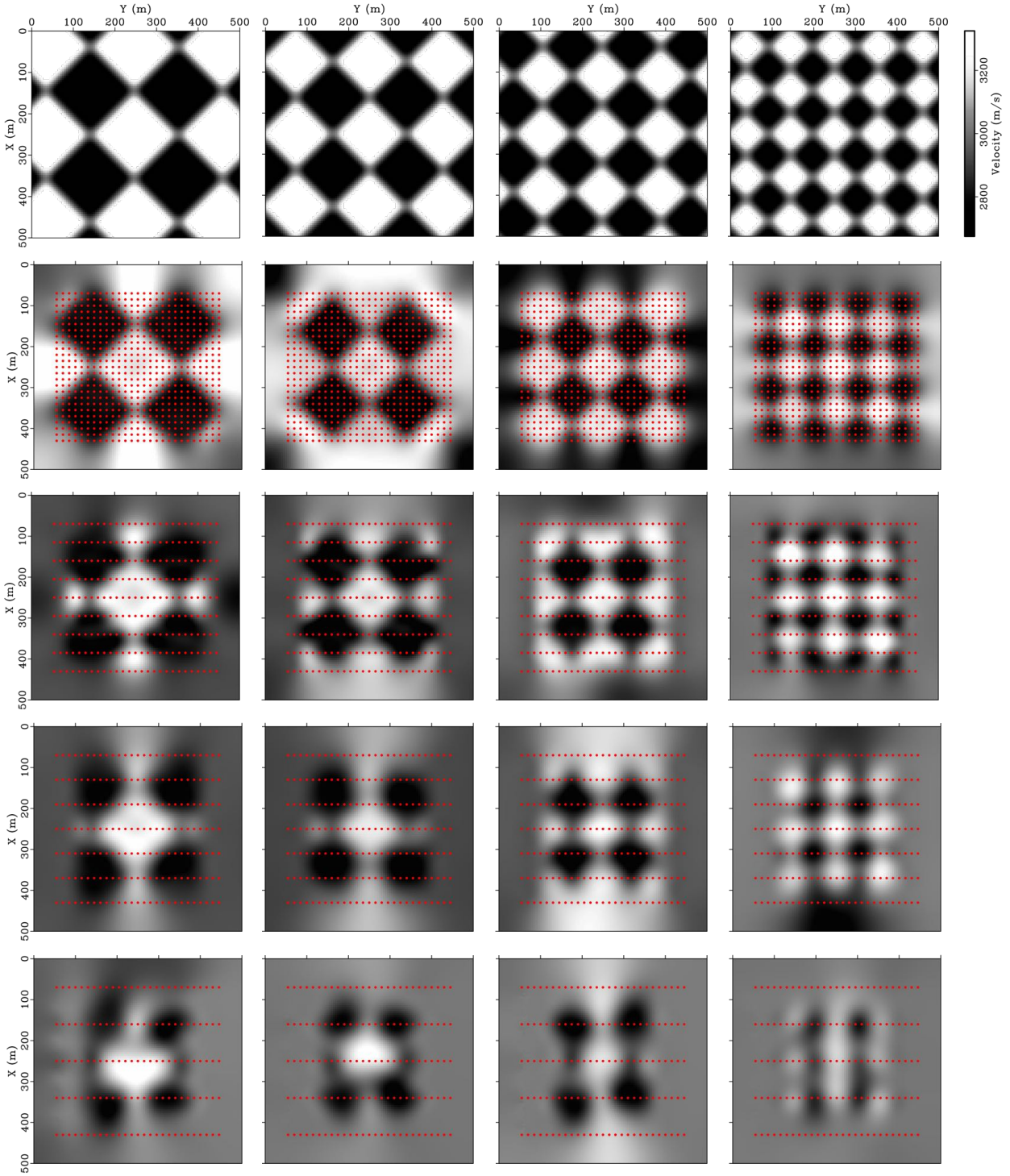

Figure 8. A series of checker board pattern experiments exploring different observation receiver geometries (rows) and varying checker sizes (columns). The receiver cross-line spacing varies as (top to bottom) 15 m, 45 m, 60 m, and 90 m. The checker sizes vary as (left to right) 75 m, 100 m, 125 m, and 150 m. True velocity models in the top row, recovered final velocity models after inversion in the rows below. Red dots indicate the observation receiver locations.

can exist and go unobserved at the station locations (which then lie at the nodes of those wave modes). An example of such wave-modes can be observed in Fig. 4a.

In the interior of the array, few wave-modes that obey a spurious velocity could go unobserved. In the limit case where the observations are very dense and approach spatially and temporally continuous observation of the wave field. No long wavelength spurious wave-modes can go unobserved and the only wave modes we can invert that match the observations compose the best estimate of the true wave field, the best fit medium parameters follow by WEI.

The wavefield reconstruction step reconstructs the wavefield in a boundary zone beyond the edges of the array. We defined a second interior domain for the wave equation step to exclude the wavefield values in this boundary zone. This may not be required. A possible alternative may be to evaluate the spatial derivatives using non-central finite differences when approaching the boundaries. This would have omitted all points in the boundary zone from the wave field reconstruction, and wave equation inversion. However, it remains to be seen if using both non-central finite differences and central finite difference for different portions of the domain may lead to other difficulties, such as stability errors or approximation errors.

Near the edges of the array, many different mode-oscillations can exist and go unobserved. A superposition of these modes could explain the observations and therefore appear in the wave field reconstruction step. The wave field reconstruction-step will result in a spurious wave-field near the edges (but inside) the array, where the observations are more sparse. This spurious wavefield deviates significantly from the unknown true wavefield but matches the sparse observations. But the spurious wavefield conforms fully with the estimated medium parameters used for the wavefield reconstruction. Consequently, the unknown true medium parameters near the edges of the array are poorly constrained by the data. The regularization term in WEI determines the recovered velocity near the edges of the array.

Ideally, we design experiments where the station geometry constrains as many wave modes as possible. The wave modes depend on the medium parameters, and a complex model may make this problem easier. It may be that random sample locations are helpful to suppress spurious wave modes that have a regularity such as the wave mode in Fig. 4a. However, such spurious wave

545 modes in the reconstructed wavefield do not bias the update for the medium parameters in an
546 erronous way, because these spurious wavemodes obey the medium parameters that were used to
547 reconstruct the wavefield.

548 The computation of matrix inverses in this study were done using LU decomposition. Conse-
549 quently, the matrices had to be full rank. This is why we inserted a wave field prior term (with a
550 very small weighting in the norm). We have verified that inversion methods such as conjugate gra-
551 dient methods work with explicitly singular matrices. Theoretically, conjugate gradient methods
552 could be run until absolute convergence and solve singular the inverse problem without regularisa-
553 tion (the null-space filled with elements inherited from the starting model). In practice, truncation
554 of the conjugate gradient iterations results in an implicit regularization.

555 The strategy for inverting ambient seismic noise in this paper can be further adapted to a host
556 of different scenarios by adapting the boundary conditions imposed on the PDE system in the
557 constraint term. For example, portions of the boundary could be made absorbing to invert for non-
558 ominidirectional wave fields such as microseism noise near coasts, or oil platform generated noise.
559 The sub domain could be constructed to exclude a known physical source location. Similarly,
560 the information contained by the wave field values in the boundary zone may be of interest to
561 characterise the medium or sources outside the sub domain. Finally, instead of inverting for wave
562 field values in a boundary zone, proper boundary conditions could be constructed as unknowns in
563 the inverse problem and inverted for.

564 A disadvantage of the joint inversion for wave field and medium parameters, is the memory
565 requirements. Especially for the case of controlled source seismic data with hundreds of separate
566 experiments, the memory requirements may be prohibitive. However, for ambient seismic datasets,
567 only one wave field needs to be reconstructed (although the recording time may be longer). Am-
568 bient seismic is naturally blended data, and the results in this paper suggest that controlled source
569 data could be blended together to reduce the number of wave fields that needs to be reconstructed.
570 The fundamental advantage sterns from the use of WEI to find an update in the medium param-
571 eters. WEI does not suffer from cross-terms between sources. Moreover, when WEI is used to

compute the gradient we avoid all errors due to approximations made in the commonly used Born linearisation of the wave equation.

8 CONCLUSIONS

We presented a new algorithm for full wave field inversion. The algorithm inverts observations of a wave field using the governing PDE system as a soft constraint, simultaneously inverting for a full reconstructed wave field and the underlying medium parameters. We formulated an algorithm in which the PDE system does require a unique solution. The boundary conditions of the wave field do not need to be specified, and can remain unknown. Therefore, this algorithm is ideally suited for inversions of ambient seismic noise recorded by large spatially dense arrays. This approach to inversion may be of use to a number of inversion challanges with poor source control but with dense sensor coverage, for example (blended source) controlled-source seismology, inverting rock properties inside laboratory samples, or even inverting the Earth's free oscillations on a global scale (normal mode seismology).

9 ACKNOWLEDGMENTS

SdR acknowledges Biondo Biondi, for his key input in a series of discussions conducted during a visit of SdR supported by the Chevron CORE at Stanford, and without whom this project would not have come to fruition. SdR is grateful to Andrew Curtis, who supported SdR first coming to the University of Edinburgh, and for many discussions and suggestions valuable for the development of this work. SdR thanks the School of Mathematics for financial support through a Whittaker Fellowship. JRM acknowledges funding from the UK Natural Environment Research Council (NE/L005166/1). We thank Ali Shaiban, who helped verify the efficacy of the conjugate gradient optimisation method, and the members of the Applied and Computational Mathematics group at the University of Edinburgh for helpful discussions and suggestions. We thank two anonymous reviewers whose comments helped to improve this manuscript.

REFERENCES

Aki, K., 1957. Space and time spectra of stationary stochastic waves, with special reference to microtremors, *Bulletin of the Earthquake Research Institute*, **35**, 415–456.

599 Aki, K. & Richards, P. G., 2002. *Quantitative Seismology*, University Science Books, 2nd edn.

600 Aster, R. C., Thurber, C. H., & Borchers, B., 2005. *Parameter Estimation and Inverse Problems*, no. v.1
601 in International geophysics series, Elsevier Academic Press.

602 Baysal, E., Kosloff, D. D., & Sherwood, J. W. C., 1983. Reverse time migration, *Geophysics*, **48**(11),
603 1514–1524.

604 Claerbout, J. F., 1968. Synthesis of a layered medium from its acoustic transmission response, *Geophysics*,
605 **33**(2), 264–269.

606 Curtis, A. & Robertsson, J. O. A., 2002. Volumetric wavefield recording and wave equation inversion for
607 near-surface material properties, *Geophysics*, **67**(5), 1602–1611.

608 de Ridder, S. & Curtis, A., 2017. Seismic gradiometry using ambient seismic noise in an anisotropic earth,
609 *Geophysical Journal International*, **209**(2), 1168–1179.

610 de Ridder, S. A. L. & Biondi, B. L., 2015. Near-surface scholte wave velocities at ekofisk from short
611 noise recordings by seismic noise gradiometry, *Geophysical Research Letters*, **42**(17), 7031–7038,
612 2015GL065027.

613 Edme, P. & Yuan, S., 2016. Local dispersion curve estimation from seismic ambient noise using spatial
614 gradients, *Interpretation*, **4**(3), SJ17.

615 Fichtner, A., 2015. Source-structure trade-offs in ambient noise correlations, *Geophysical Journal Inter-*
616 *national*, **202**(1), 678.

617 Hudson, J. A. & Heritage, J. R., 1981. The use of the born approximation in seismic scattering problems,
618 *Geophysical Journal of the Royal Astronomical Society*, **66**(1), 221–240.

619 Langston, C. A., 2007. Spatial gradient analysis for linear seismic arrays, *Bulletin of the Seismological*
620 *Society of America*, **97**(1B), 265–280.

621 LeBras, R. & Clayton, R. W., 1988. An iterative inversion of back-scattered acoustic waves, *Geophysics*,
622 **53**(4), 501–508.

623 Liang, C. & Langston, C. A., 2009. Wave gradiometry for USArray: Rayleigh waves, *Journal of Geophys-*
624 *ical Research: Solid Earth*, **114**(B2), n/a–n/a.

625 Liu, Y. & Holt, W. E., 2015. Wave gradiometry and its link with helmholtz equation solutions ap-
626 plied to usarray in the eastern u.s., *Journal of Geophysical Research: Solid Earth*, **120**(8), 5717–5746,
627 2015JB011982.

628 Lobkis, O. I. & Weaver, R. L., 2001. On the emergence of the green's function in the correlations of a
629 diffuse field, *J. Acoust. Soc. Am.*, **110**(6), 3011–3017.

630 Plessix, R.-E., 2006. A review of the adjoint-state method for computing the gradient of a functional with
631 geophysical applications, *Geophysical Journal International*, **167**(2), 495–503.

632 Poppeliers, C., Punoševac, P., & Bell, T., 2013. Three-dimensional seismic-wave gradiometry for scalar
633 waves, *Bulletin of the Seismological Society of America*, **103**(4), 2151–2160.

Rickett, J., 2013. The variable projection method for waveform inversion with an unknown source function, *Geophysical Prospecting*, **61**(4), 874–881.

Sager, K., Ermert, L., Boehm, C., & Fichtner, A., 2018. Towards full waveform ambient noise inversion, *Geophysical Journal International*, **212**(1), 566–590.

Snieder, R., Slob, Y. F. E., & Wapenaar, K., 2010. Equipartitioning is not sufficient for green's function extraction, *Earthquake Science*, **23**, 403–415.

Tarantola, A., 1984. Inversion of seismic reflection data in the acoustic approximation, *Geophysics*, **49**(8), 1259–1266.

Tarantola, A., 2005. *Inverse Problem Theory and Methods for Model Parameter Estimation*, Society for Industrial and Applied Mathematics.

Tromp, J., Luo, Y., Hanasoge, S., & Peter, D., 2010. Noise cross-correlation sensitivity kernels, *Geophysical Journal International*, **183**(2), 791–819.

van Leeuwen, T. & Herrmann, F. J., 2013. Mitigating local minima in full-waveform inversion by expanding the search space, *Geophysical Journal International*, **195**(1), 661–667.

Wapenaar, K. & Fokkema, J., 2006. Green's function representations for seismic interferometry, *Geophysics*, **71**(4), SI33–SI46.

Wunsch, C., 2006. *Discrete Inverse and State Estimation Problems: With Geophysical Fluid Applications*, Cambridge University Press.

Zhan, Z., Li, Q., & Huang, J., 2018. Application of wavefield compressive sensing in surface wave tomography, *Geophysical Journal International*, **213**(3), 1731–1743.

Appendix A: Formulation

Consider a Fréchet differentiable Lagrange constrained function $\mathcal{L} : V_u \times V_m \times V_s \times V_{\breve{\lambda}} \rightarrow \mathbb{R}$ with

$$\mathcal{L}\left(u, m, s, \lambda\right) = E_u\left(u\right) + E_m\left(m\right) + E_s\left(s\right) - \left\langle \breve{\lambda}, \mathcal{F}\left(u, m\right) - s \right\rangle_{L^2}, \tag{31}$$

where $E_u : V_u \rightarrow \mathbb{R}$, $E_m : V_m \rightarrow \mathbb{R}$, $E_s : V_s \rightarrow \mathbb{R}$, and $\mathcal{F} : V_u \times V_m \rightarrow V_F$ are given functions. $V_u, V_m, V_{\breve{\lambda}}, V_F \subseteq L^2\left(\Omega; \mathbb{R}\right)$ are Hilbert spaces, where $\Omega \subseteq \left(\mathbb{R}^d, \mathbb{R}\right)$ is an open, bounded, and appropriately regular domain corresponding to a 'space-time' domain with d spatial dimensions and one time dimension. V_s is an affine space defined so that $V_s = \{s_0 + s_1 : s_0 \in V_{s,0}\}$, where $s_1 \in L^2\left(\Omega; \mathbb{R}\right)$ is given (and typically equal to a given 'prior' s_p) and $V_{s,0}$ is a Hilbert space. V_u is the search space for the wave-field, V_m is the search space for the medium parameters, V_s is the search space for the excitation, and $\mathcal{F}\left(u, m\right) - s$ is the residual of one or more partial differential

equations given the wave-field u, medium parameters m, and excitation s.

At a stationary point of $\mathcal{L}$ it follows (by differentiating with respect to $\breve{\lambda}$) that

$$\left\langle \zeta, \mathcal{F}\left(u,m\right) - s \right\rangle_{L^2} = 0 \quad \forall \zeta \in V_{\breve{\lambda}}, \tag{32}$$

which expresses the imposition of the Lagrange constraint. If $V_{s,0} \subseteq V_\lambda$ then this implies

$$\left\langle \zeta, s \right\rangle_{L^2} = \left\langle \zeta, \mathcal{F}\left(u,m\right) \right\rangle_{L^2} \quad \forall \zeta \in V_{s,0}, \tag{33}$$

and, since in this case $s_0 = s - s_1 \in V_{s,0} \subseteq V_{\breve{\lambda}}$, then this implies that at a stationary point of $\mathcal{L}$ the excitation s is the Galerkin L^2 projection (i.e. the L^2 optimal projection) of $\mathcal{F}\left(u,m\right)$ onto V_s. This is denoted

$$s = \Psi_{L^2}\left(\mathcal{F}\left(u,m\right)\right), \tag{34}$$

where $\Psi_{L^2} : V_F \to V_s$ is the operator expressing the Galerkin L^2 projection of an element of V_F onto V_s. In this case a new function $\widehat{\mathcal{L}} : V_u \times V_m \to \mathbb{R}$ may be defined where

$$\widehat{\mathcal{L}}\left(u,m\right) = E_u\left(u\right) + E_m\left(m\right) + E_s\left(\Psi_{L^2}\left(\mathcal{F}\left(u,m\right)\right)\right). \tag{35}$$

Assuming $\widehat{\mathcal{L}}$ is Fréchet differentiable, we seek a stationary point $\left(u_0, m_0\right)$ of this new functional.

In the examples considered in this article E_u incorporates the mis-match between the wave field and observational data, and also a regularisation penalising the magnitude of the wave field

$$E_u\left(u\right) = \frac{1}{2N}\left\|\Pi_u\left(u\right) - \mathbf{u}_d\right\|_2^2 + \frac{1}{2}\left\|\epsilon_2 u\right\|_{L^2}^2. \tag{36}$$

Here $\Pi_u : V_u \to \mathbb{R}^N$ is a 'sampling operator', yielding values for the wave field at the locations at which N observations in the vector $\mathbf{u}_d \in \mathbb{R}^N$ are available. E_m incorporates a regularision penalising deviations from a given 'prior' field $m_p \in L^2\left(\Omega;\mathbb{R}\right)$, and penalising non-smooth deviations from this prior, via

$$E_m\left(m\right) = \frac{1}{2}\left\|\epsilon_3 \nabla^2\left[m - m_p\right]\right\|_{L^2}^2 + \frac{1}{2}\left\|\epsilon_4\left[m - m_p\right]\right\|_{L^2}^2, \tag{37}$$

where the Laplacian appearing here (and in the following equations) may be replaced with an appropriate weak version depending on the regularity of $m - m_p$. E_s incorporates a regularisation

penalising the magnitude of the excitation

$$E_s(u) = \frac{1}{2}\left\|\epsilon_1 s\right\|_{L^2}^2, \tag{38}$$

thereby penalising the degree to which the wave field deviates from a solution which solves the unforced wave equation. In the above $\epsilon_1, \epsilon_2, \epsilon_3, \epsilon_4 \in L^2(\Omega;\mathbb{R})$ are appropriate weighting functions. The function $\mathcal{F}$ represents a weak form of the wave equation. If no initial, terminal, or boundary conditions are applied to the wave-field, with $V_u \subseteq H^1(\Omega;\mathbb{R})$ and $V_\lambda \subseteq H_0^1(\Omega;\mathbb{R})$, then $\mathcal{F}$ may be defined by choosing $V_F = V_{\breve{\lambda}}$, and with

$$\left\langle \zeta, \mathcal{F}(u,m)\right\rangle_{L^2} = -\left\langle \frac{\partial \zeta}{\partial t}, \frac{\partial u}{\partial t}\right\rangle_{L^2} + \left\langle \nabla(\zeta m), \nabla u\right\rangle_{L^2} \quad \forall \zeta \in V_F = V_\lambda. \tag{39}$$

Moreover if $V_{s,0} \subseteq V_{\breve{\lambda}}$ then

$$\left\langle \zeta, \Psi_{L^2}(\mathcal{F}(u,m))\right\rangle_{L^2} = -\left\langle \frac{\partial \zeta}{\partial t}, \frac{\partial u}{\partial t}\right\rangle_{L^2} + \left\langle \nabla(\zeta m), \nabla u\right\rangle_{L^2} \quad \forall \zeta \in V_{s,0}. \tag{40}$$

Gathering the above definitions and results, a Lagrange constrained function $\mathcal{L} : V_u \times V_m \times V_s \times V_{\breve{\lambda}} \to \mathbb{R}$ of the following form is considered

$$\begin{aligned}\mathcal{L}\left(u,m,s,\breve{\lambda}\right) = \frac{1}{2N}\left\|\Pi_u(u) - \mathbf{u}_d\right\|_2^2 + \frac{1}{2}\left\|\epsilon_1 s\right\|_{L^2}^2 + \frac{1}{2}\left\|\epsilon_2 u\right\|_{L^2}^2 + \frac{1}{2}\left\|\epsilon_3 \nabla^2 [m - m_p]\right\|_{L^2}^2 \\ + \frac{1}{2}\left\|\epsilon_4 [m - m_p]\right\|_{L^2}^2 \\ + \left\langle \frac{\partial \breve{\lambda}}{\partial t}, \frac{\partial u}{\partial t}\right\rangle_{L^2} - \left\langle \nabla\left(\breve{\lambda} m\right), \nabla u\right\rangle_{L^2} + \left\langle \breve{\lambda}, s\right\rangle_{L^2},\end{aligned} \tag{41}$$

with $V_u \subseteq H^1(\Omega;\mathbb{R})$ and $V_\lambda \subseteq H_0^1(\Omega;\mathbb{R})$ so that no initial, terminal, or boundary conditions are applied for the wave-field. Taking $s_1 = 0$, if $V_s = V_{s,0} \subseteq V_\lambda$, implying in particular that s vanishes on the space-time boundary at a stationary point, then the problem of seeking stationary points of $\mathcal{L}$ can be replaced with the problem of seeking stationary points of $\widehat{\mathcal{L}} : V_u \times V_m \to \mathbb{R}$ where

$$\begin{aligned}\widehat{\mathcal{L}}(u,m) = \frac{1}{2N}\left\|\Pi_u(u) - \mathbf{u}_d\right\|_2^2 + \frac{1}{2}\left\|\epsilon_1 \Psi_{L^2}(\mathcal{F}(u,m))\right\|_{L^2}^2 + \frac{1}{2}\left\|\epsilon_2 u\right\|_{L^2}^2 + \frac{1}{2}\left\|\epsilon_3 \nabla^2 [m - m_p]\right\|_{L^2}^2 \\ + \frac{1}{2}\left\|\epsilon_4 [m - m_p]\right\|_{L^2}^2,\end{aligned} \tag{42}$$

with $\Psi_{L^2}(\mathcal{F}(u,m))$ given by Eq. 40.

Appendix B: Discretisation

If a Galerkin finite element or Galerkin spectral discretisation is applied, then a discrete version of the optimisation problem described in Appendix A is obtained immediately: one restricts V_u, V_m, and $V_{s,0}$ to be appropriate Hilbert spaces each of which have a finite basis.

Here instead a finite difference discretisation for this problem is considered, with a regular structured spatial grid with spacing Δx in each spatial dimension, and spacing Δt in the time dimension. The medium parameter m is allowed to vary only in space, and other fields are permitted to be functions of both space and time. Let there be n points in the full discrete space-time grid, with $n - p$ points associated with space-time boundary points. Let there be q points in the spatial grid. The discrete approximations for the wave field u and source s then have n degrees of freedom, and the discrete approximation for the medium parameter m has q degrees of freedom. For simplicity each of the ϵ_i are here assumed to be non-negative constants. A discrete version of the optimisation problem is formulated by seeking $\mathbf{u}_0, \mathbf{s}_0 \in \mathbb{R}^n$, $\mathbf{m}_0 \in \mathbb{R}^q$, and $\breve{\boldsymbol{\lambda}}_0 \in \mathbb{R}^p$, such that $\mathcal{L}^\delta : \mathbb{R}^n \times \mathbb{R}^q \times \mathbb{R}^n \times \mathbb{R}^p \to \mathbb{R}$ where

$$\begin{aligned}\mathcal{L}^\delta\left(\mathbf{u}, \mathbf{m}, \mathbf{s}, \breve{\boldsymbol{\lambda}}\right) = \frac{1}{2N}\left\|\mathbf{K}\mathbf{u} - \mathbf{d}\right\|_2^2 + \frac{1}{2}\Delta t \Delta x^d \left[\epsilon_1^2 \left\|\mathbf{s}\right\|_2^2 + \epsilon_2^2 \left\|\mathbf{u}\right\|_2^2 + \epsilon_3^2 \left\|\mathbf{L}\left(\mathbf{P}\mathbf{m} - \mathbf{m}_p\right)\right\|_2^2\right. \\ \left. + \epsilon_4^2 \left\|\mathbf{P}\mathbf{m} - \mathbf{m}_p\right\|_2^2\right] - \\ \Delta t \Delta x^d \breve{\boldsymbol{\lambda}}^T \left(\breve{\mathbf{D}}\mathbf{u} - \breve{\mathbf{I}}\,\mathrm{diag}\left\{\mathbf{P}\mathbf{m}\right\}\,\breve{\mathbf{I}}^T\breve{\mathbf{L}}\mathbf{u} - \breve{\mathbf{I}}\mathbf{s}\right),\end{aligned} \tag{43}$$

is stationary. This is a finite difference discretised version of $\mathcal{L}$ in Eq. 41. Here $\mathbf{K}$ is an $N \times n$ matrix corresponding to the evaluation of the discrete wave field at the observation points. $\mathbf{L}$ is a real $n \times n$ matrix corresponding to a discretisation of ∇^2, $\breve{\mathbf{D}}$ is a real $p \times n$ matrix corresponding to a discretisation of $\partial^2/\partial t^2$ on the interior of the space-time domain, and $\breve{\mathbf{L}}$ is a real $p \times n$ matrix corresponding to a discretisation of ∇^2 on the interior of the space-time domain. $\breve{\mathbf{I}}$ is a $p \times n$ matrix equal to an identity matrix with rows corresponding to the space-time boundary points removed. $\mathbf{P}$ is a real $n \times q$ matrix which yields values for the medium parameter on the full space-time grid. $\mathbf{m}_\mathrm{p} \in \mathbb{R}^n$ corresponds to m_p interpolated onto the numerical grid. Given a $\mathbf{v} \in \mathbb{R}^r$, $\mathrm{diag}\left\{\mathbf{v}\right\}$ is an $r \times r$ diagonal matrix whose i^{th} diagonal element is equal to the ith element of the vector $\mathbf{v}$. The factors of $\Delta t \Delta x^d$ are the grid point volumes which arise from a discretised version of the

L^2 norm and inner product. More generally additional weighting matrices can be introduced to, for example, take account of the reduced volume associated with grid points on the space-time boundary points, or for the use of non-uniform grids.

Differentiating and seeking stationary points leads to the following non-linear system

$$\left[\frac{1}{N\Delta t\Delta x^d}\mathbf{K}^T\mathbf{K}+\epsilon_2^2\mathbf{I}\right]\mathbf{u}-\left(\breve{\mathbf{D}}-\breve{\mathbf{I}}\,\mathrm{diag}\left\{\mathbf{P}\mathbf{m}\right\}\,\breve{\mathbf{I}}^T\breve{\mathbf{L}}\right)^T\breve{\boldsymbol{\lambda}}=\frac{1}{N\Delta t\Delta x^d}\mathbf{K}^T\mathbf{d}, \tag{44a}$$

$$\mathbf{P}^T\,\mathrm{diag}\left\{\breve{\mathbf{I}}^T\breve{\mathbf{L}}\mathbf{u}\right\}\,\breve{\mathbf{I}}^T\breve{\boldsymbol{\lambda}}+\left(\epsilon_3^2\mathbf{P}^T\mathbf{L}^T\mathbf{L}\mathbf{P}+\epsilon_4^2\mathbf{P}^T\mathbf{P}\right)\mathbf{m}=\left(\epsilon_3^2\mathbf{P}^T\mathbf{L}^T+\epsilon_4^2\mathbf{P}^T\right)\mathbf{m}_\mathrm{p}, \tag{44b}$$

$$\epsilon_1^2\mathbf{s}+\breve{\mathbf{I}}^T\breve{\boldsymbol{\lambda}}=\mathbf{0}, \tag{44c}$$

$$\breve{\mathbf{I}}\mathbf{s}=\breve{\mathbf{D}}\mathbf{u}-\breve{\mathbf{I}}\,\mathrm{diag}\left\{\mathbf{P}\mathbf{m}\right\}\,\breve{\mathbf{I}}^T\breve{\mathbf{L}}\mathbf{u}, \tag{44d}$$

where $\mathbf{I}$ is an $n\times n$ identity matrix, and the use of $\{\}_0$ to denote a stationary point is now omitted. The fourth equation here is a finite difference discretised version of $\Psi_{L^2}\left(\mathcal{F}\left(u,m\right)\right)$ in Eq. 40 – with the excitation allowed to be vary at each point in the space-time grid (noting that if $\epsilon_1\neq 0$ the third equation here implies that $\mathbf{s}$ vanishes on space-time boundary points), and with this finite difference discretisation, the discretised version of $\Psi_{L^2}\left(\mathcal{F}\left(u,m\right)\right)$ takes a particularly simple form. Assuming $\epsilon_1\neq 0$, the third equation allows $\breve{\mathbf{I}}\mathbf{s}$ to be eliminated which, using the fourth equation, allows the Lagrange multiplier $\breve{\boldsymbol{\lambda}}$ to be eliminated

$$\breve{\mathbf{I}}\mathbf{s}=-\frac{1}{\epsilon_1^2}\breve{\boldsymbol{\lambda}}, \tag{45a}$$

$$\breve{\boldsymbol{\lambda}}=-\epsilon_1^2\left(\breve{\mathbf{D}}\mathbf{u}-\breve{\mathbf{I}}\,\mathrm{diag}\left\{\mathbf{P}\mathbf{m}\right\}\,\breve{\mathbf{I}}^T\breve{\mathbf{L}}\mathbf{u}\right). \tag{45b}$$

759 The discrete constrained least-squared non-linear optimisation problem is thus a solution of

$$\left[\frac{1}{N\Delta t\Delta x^d}\mathbf{K}^T\mathbf{K} + \epsilon_2^2\mathbf{I} + \epsilon_1^2\left(\breve{\mathbf{D}} - \breve{\mathbf{I}}\,\mathrm{diag}\left\{\mathbf{P}\mathbf{m}\right\}\,\breve{\mathbf{I}}^T\breve{\mathbf{L}}\right)^T\left(\breve{\mathbf{D}} - \breve{\mathbf{I}}\,\mathrm{diag}\left\{\mathbf{P}\mathbf{m}\right\}\,\breve{\mathbf{I}}^T\breve{\mathbf{L}}\right)\right]\mathbf{u} = \tag{46a}$$

$$\frac{1}{N\Delta t\Delta x^d}\mathbf{K}^T\mathbf{d},$$

$$\left[\epsilon_1^2\mathbf{P}^T\,\mathrm{diag}\left\{\breve{\mathbf{I}}^T\breve{\mathbf{L}}\mathbf{u}\right\}\,\breve{\mathbf{I}}^T\breve{\mathbf{I}}\,\mathrm{diag}\left\{\breve{\mathbf{I}}^T\breve{\mathbf{L}}\mathbf{u}\right\}\,\mathbf{P} + \epsilon_3^2\mathbf{P}^T\mathbf{L}^T\mathbf{L}\mathbf{P} + \epsilon_4^2\mathbf{P}^T\mathbf{P}\right]\mathbf{m} = \tag{46b}$$

$$\left(\epsilon_3^2\mathbf{P}^T\mathbf{L}^T + \epsilon_4^2\mathbf{P}^T\right)\mathbf{m}_\mathrm{p} + \epsilon_1^2\mathbf{P}^T\,\mathrm{diag}\left\{\breve{\mathbf{I}}^T\breve{\mathbf{L}}\mathbf{u}\right\}\,\breve{\mathbf{I}}^T\breve{\mathbf{D}}\mathbf{u}.$$

764 (46c)

765 This is a finite difference discretised version of the equations for a stationary point of $\widehat{\mathcal{L}}$ in Eq. 42.